Biophysical Journal
Article

Biophysical Society

Revising Berg-Purcell for finite receptor kinetics

Gregory Handy[1,2] and Sean D. Lawley[3,*]
[1]Departments of Neurobiology and Statistics and [2]Grossman Center for Quantitative Biology and Human Behavior, University of Chicago, Chicago, Illinois; and [3]Department of Mathematics, University of Utah, Salt Lake City, Utah

ABSTRACT From nutrient uptake to chemoreception to synaptic transmission, many systems in cell biology depend on molecules diffusing and binding to membrane receptors. Mathematical analysis of such systems often neglects the fact that receptors process molecules at finite kinetic rates. A key example is the celebrated formula of Berg and Purcell for the rate that cell surface receptors capture extracellular molecules. Indeed, this influential result is only valid if receptors transport molecules through the cell wall at a rate much faster than molecules arrive at receptors. From a mathematical perspective, ignoring receptor kinetics is convenient because it makes the diffusing molecules independent. In contrast, including receptor kinetics introduces correlations between the diffusing molecules because, for example, bound receptors may be temporarily blocked from binding additional molecules. In this work, we present a modeling framework for coupling bulk diffusion to surface receptors with finite kinetic rates. The framework uses boundary homogenization to couple the diffusion equation to nonlinear ordinary differential equations on the boundary. We use this framework to derive an explicit formula for the cellular uptake rate and show that the analysis of Berg and Purcell significantly overestimates uptake in some typical biophysical scenarios. We confirm our analysis by numerical simulations of a many-particle stochastic system.

SIGNIFICANCE Many systems in cell biology involve molecules diffusing and binding to membrane receptors. To simplify analysis, mathematical models of these systems often assume that receptors can process molecules at infinite kinetic rates. Including finite receptor kinetics is challenging because it means the diffusive molecules are no longer noninteracting, as they affect each other through their interactions with receptors. In this work, we present a modeling framework for coupling diffusion to surface receptors with finite kinetic rates. We use this framework to show that an influential analysis of Berg and Purcell significantly overestimates the rate that a cell can capture extracellular molecules in some typical biophysical scenarios.

INTRODUCTION

Many biological systems depend on molecules diffusing and interacting with membrane receptors. For example, cellular nutrient uptake relies on cell surface receptors binding and transporting diffusing molecules into the cell (1). Chemoreception and chemotaxis similarly depend on cell surface receptors binding extracellular diffusing molecules (2). An important part of the immune response involves antibodies binding to epitopes on the surface of a virion (3,4). In addition, synaptic transmission requires neurotransmitter molecules released from one neuron to diffuse across the synaptic cleft and bind to receptors on the adjacent neuron (5).

In most instances, the receptors cannot bind molecules continuously, but rather binding one or more molecules temporarily hinders binding additional molecules (see Fig. 1 for an illustration). This could be due simply to mutual exclusion at the receptor (i.e., a receptor can only bind one molecule at a time). Alternatively, this effect could be due to the finite rate that a receptor can transport bound molecules into the cell, as in the case of nutrient transport (6,7). Similarly, the effect could stem from a finite receptor internalization rate (8–10). In the case of synaptic transmission, a receptor that captures a molecule changes conformation, and during this time it cannot capture additional molecules (5,11,12). That is, the receptor must wait a transitory "recharge" time after the capture of any molecule before additional captures. A similar recharge time affects experiments in which molecules are released into extracellular space in the brain and bind to receptors on astrocytes (13). In ecology, this notion of a recharge time is called the handling time, and it is the time a predator (the

Submitted December 15, 2020, and accepted for publication March 25, 2021.

*Correspondence: lawley@math.utah.edu

Editor: Ramon Grima.
https://doi.org/10.1016/j.bpj.2021.03.021

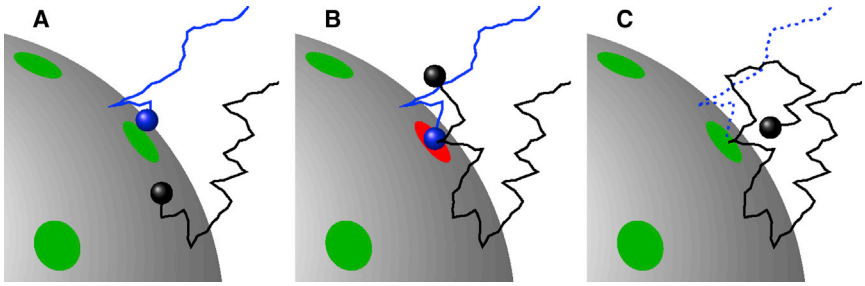

FIGURE 1 (*a*) The blue and black molecules compete to bind to a surface receptor. (*b*) The blue molecule binds to a receptor. The black molecule is then temporarily blocked from binding to that receptor. (*c*) After some time, the blue molecule is absorbed by the receptor, and that receptor is free to bind the black molecule. To see this figure in color, go online.

"receptor") must wait after capturing a prey (the "molecule") before it can hunt again.

The common feature of these examples is that the receptors process molecules at finite kinetic rates. Mathematical models often neglect receptor kinetics, which greatly simplifies the analysis because it allows the diffusing molecules to be independent. Including receptor kinetics makes the diffusing molecules dependent, as the molecules may affect each other through their interactions with the receptors. For example, if one molecule binds to a receptor, then additional molecules may be temporarily blocked from that receptor.

An important example of mathematical analysis that neglects receptor kinetics is the formula of Berg and Purcell for the rate that cell surface receptors capture extracellular molecules (2). Assuming that the receptors occupy a small fraction of the cell surface, they found that the uptake rate is

$$J_{\mathrm{bp}} := \frac{\varepsilon N}{\varepsilon N + \pi} J_{\max}, \tag{1}$$

where ε is the ratio of the receptor radius to the cell radius, $N \geq 1$ is the number of receptors, and $J_{\max}$ is the uptake rate if the entire surface is covered by perfectly absorbing receptors (2). In particular, $J_{\max}$ is (14)

$$J_{\max} := 4\pi D R u_0, \tag{2}$$

where R is the cell radius, D is the diffusivity of extracellular molecules, and u_0 is the concentration of extracellular molecules.

Berg and Purcell's formula in Eq. 1 has been very influential. Indeed, many works have sought to refine Eq. 1 to incorporate the effects of other details in the problem. For example, Zwanzig used an effective medium formalism to account for the effects of interference between receptors (15). Other works have modified Eq. 1 to include other effects, including receptor arrangement, cell membrane curvature, and receptor motion (16–26). In one particularly important study, Wagner et al. (27) extended Eq. 1 to nonspherical geometries and used this analysis to argue that the cylindrical morphology of cell envelope extensions serves to increase nutrient uptake.

To derive Eq. 1, Berg and Purcell (2) assumed that any molecule that touches a receptor "is immediately (or within a time short compared to the interval between arrivals) captured and transported through the cell wall, clearing the site for its next catch."
This assumption makes the diffusing molecules independent. However, it is clear that this assumption is violated at sufficiently high extracellular concentrations.

In this work, we present a modeling framework for coupling bulk diffusion of molecular species to surface receptors with finite kinetics. Mathematically, this framework uses boundary homogenization to link the diffusion equation (a partial differential equation (PDE)) to boundary conditions described by nonlinear ordinary differential equations (ODEs). We then reduce this PDE-ODE system to a PDE with a nonlinear boundary condition of Michaelis-Menten type. We confirm the predictions of this framework and analysis with detailed numerical simulations of a full, many-particle stochastic system. Although the general framework can be applied in a variety of problems and geometries, we develop the theory primarily in the context of the Berg-Purcell problem described above. We derive an explicit formula for the cellular uptake rate as a function of the various parameters in the problem, including the kinetic rates of receptors. We show that the classical result in Eq. 1 significantly overestimates uptake in some typical biophysical scenarios.

The rest of the study is organized as follows. We first rederive the classical result in Eq. 1, and then we present the PDE-ODE framework and derive a reduced Michaelis-Menten boundary condition. Next, we use the modeling framework to find explicit formulas for various steady-state quantities, including cellular uptake and the fraction of bound receptors. We then describe our numerical methods and verify the predictions of the modeling framework by stochastic simulations. Finally, we explore some biophysical implications of our results in typical parameter regimes of interest. We conclude by discussing related work and highlighting future directions.

METHODS

Berg-Purcell and boundary homogenization

We begin by reviewing the model of Berg and Purcell (2) and boundary homogenization (17,19,23,28–30). Consider a spherical cell in a large medium containing spherical molecules of some substrate. Fixing our

reference frame on the cell, the substrate concentration, $u = u(r, \theta, \varphi, t)$, satisfies the diffusion equation in spherical coordinates (r, θ, φ),

$$\frac{\partial}{\partial t}u = D\Delta u, \quad r > R, \tag{3}$$

where $D > 0$ is the substrate diffusivity and $R > 0$ is the cell radius. The concentration is held constant far from the cell,

$$\lim_{r\to\infty} u = u_0 > 0. \tag{4}$$

The cell has $N >> 1$ surface receptors for the substrate. The receptors are roughly evenly distributed on the cell surface, and each receptor is a small circular patch of radius εR with $\varepsilon << 1$. Substrate molecules can be absorbed by receptors and otherwise reflect from the cell surface. We thus have mixed boundary conditions at $r = R$,

$$\begin{aligned} D\frac{\partial}{\partial r}u &= \frac{D}{R}\kappa_{\text{rec}}u, \ r = R, \text{ and } (\theta,\varphi) \text{ in a receptor,} \\ \frac{\partial}{\partial r}u &= 0, \quad r = R, \text{ and } (\theta,\varphi) \text{ not in a receptor,} \end{aligned} \tag{5}$$

where

$$\kappa_{\text{rec}} \in (0, \infty) \cup \{\infty\}, \tag{6}$$

is a dimensionless parameter describing the rate that a receptor binds a substrate molecule. Berg and Purcell took $\kappa_{\text{rec}} = \infty$, which means that a substrate is immediately absorbed upon contact with a receptor (2). If $\kappa_{\text{rec}} = \infty$, then the first boundary condition in Eq. 5 means $u = 0$.

The method of boundary homogenization replaces the heterogeneous boundary conditions in Eq. 5 by a homogeneous boundary condition of the form

$$D\frac{\partial}{\partial r}u = \frac{D}{R}\kappa u, \quad r = R \tag{7}$$

for some dimensionless trapping rate $\kappa > 0$. The trapping rate κ is chosen to encapsulate the effective binding properties of the heterogeneous surface in Eq. 5. Notice that $\kappa << 1$ corresponds to a surface that is mostly reflecting, whereas $\kappa >> 1$ corresponds to a surface that is mostly absorbing. The benefit of boundary homogenization is that it makes the substrate concentration $u = u(r, t)$ depend only on the radius $r \geq R$ and time $t \geq 0$ and not on the angular variables (θ, φ) (assuming the initial condition is independent of (θ, φ)).

The idea behind boundary homogenization is that because of diffusion in the angular variables, the surface heterogeneity only affects the substrate concentration near the surface. In particular, the concentration is constant in the angular variables outside a boundary layer, where the width of this layer depends on the length scale of the surface heterogeneity. Many sophisticated methods have been developed to choose the trapping rate κ in Eq. 7 to incorporate the number, size, and arrangement of receptors (17–26). If the receptors occupy a small fraction of the cell surface, then the trapping rate is linear in the number of receptors N and is given by (16,19,28)

$$\kappa = \frac{\varepsilon N}{\pi}\left(1 + \frac{4}{\varepsilon\pi\kappa_{\text{rec}}}\right)^{-1}, \tag{8}$$

where $1/\kappa_{\text{rec}} = 0$ if $\kappa_{\text{rec}} = \infty$.

It is straightforward to solve Eqs. 3 and 4 and Eq. 7 at steady state to obtain the large-time substrate flux into the cell by integrating over the surface of the sphere of radius $R > 0$ (2),

$$\lim_{t\to\infty} D\int_{r=R} \tfrac{\partial}{\partial r}u \, \mathrm{d}S = \tfrac{\kappa}{\kappa+1}J_{\max}, \tag{9}$$

where $J_{\max}$ is in Eq. 2 and is the flux in the case that the entire cell surface is absorbing (14). If $\kappa_{\text{rec}} = \infty$, then Eqs. 8 and 9 yield the Berg-Purcell (2) flux formula in Eq. 1.

Including finite receptor kinetics

The model above assumes that receptors can continuously absorb substrates. That is, it assumes that there is no limit to the rate that a receptor can process substrate molecules. This modeling assumption is valid if receptors process molecules much faster than molecules tend to hit receptors.

When is a system in this parameter regime? If we use the following characteristic values (used in, for example (2)),

$$D = 10^3\ \mu\text{m}^2\text{s}^{-1}, \quad R = 1\ \mu\text{m}, \quad u_0 = 1\ \mu\text{M},$$

then molecules arrive to the cell surface at rate (see Eq. 2)

$$J_{\max} = 7.5 \times 10^6\ \text{s}^{-1}.$$

If we use the following characteristic values (again, see Berg and Purcell (2)) for the dimensionless receptor radius ε and the number of receptors N,

$$\varepsilon = 10^{-3}, \quad N = 10^3,$$

then Eq. 1 implies that the arrival rate to a single receptor is

$$\frac{J_{\text{bp}}}{N} = \frac{\varepsilon}{\varepsilon N + \pi}J_{\max} = 1.8 \times 10^3\ \text{s}^{-1}. \tag{10}$$

Hence, in this parameter regime, the Berg-Purcell formula in Eq. 1 gives a valid estimate of cellular uptake if a single receptor can transport molecules through the cell wall at a rate much faster than Eq. 10. However, the so-called turnover rates of membrane transporters are usually in the range (31)

$$k_c \in \left[3 \times 10^1, 3 \times 10^2\right]\ \text{s}^{-1},$$

which is much slower than Eq. 10.

Receptors modeled by ODEs

To model membrane receptors with finite kinetics, we suppose that the substrate molecules interact with the receptors via a classical substrate and enzyme reaction scheme,

$$S + E \underset{k_b}{\overset{k_a}{\rightleftharpoons}} C \xrightarrow{k_c} P + E. \tag{11}$$

Here, $k_a > 0$, $k_b \geq 0$, and $k_c \geq 0$ denote, respectively, the rates of "association," "breakup," and "catalysis" (32). In this formalism, freely diffusing extracellular substrates are represented by S, and the receptors play the role of the enzyme E. In particular, a substrate S diffuses and binds to a receptor E when it forms the complex C. During this time, the receptor is unavailable to bind with another substrate molecule until it "recharges" by either producing P or releasing the substrate S. The product P could represent a substrate molecule that was transported into the cell or a modified substrate molecule that was released back into the extracellular bulk but can no longer interact with receptors. Note that we allow for the possibility that $k_b = 0$ or $k_c = 0$.

Mathematically, we replace the homogenized boundary condition in Eq. 7 at the cell surface by

$$D\frac{\partial}{\partial r}u(R,t) = k_a e(t)u(R,t) - k_b c(t), \tag{12}$$

where the free receptor and bound receptor concentrations, $e(t)$ and $c(t)$, satisfy the ODEs,

$$\begin{aligned}\frac{\mathrm{d}}{\mathrm{d}t}e(t) &= -k_{\mathrm{a}}e(t)u(R,t) + (k_{\mathrm{b}}+k_{\mathrm{c}})c(t),\\ \frac{\mathrm{d}}{\mathrm{d}t}c(t) &= k_{\mathrm{a}}e(t)u(R,t) - (k_{\mathrm{b}}+k_{\mathrm{c}})c(t).\end{aligned} \tag{13}$$

Adding the equations in Eq. 13, we see that the total receptor concentration, given by the number of receptors per the surface area of the cell,

$$e_0 := \frac{N}{4\pi R^2}, \tag{14}$$

is conserved. That is, $e(t) = e_0 - c(t)$. Note that k_{a} has dimension

$$[k_{\mathrm{a}}] = (\mathrm{length})^3(\mathrm{time})^{-1},$$

whereas k_{b} and k_{c} are pure rates with dimension

$$[k_{\mathrm{b}}] = [k_{\mathrm{c}}] = (\mathrm{time})^{-1}.$$

Furthermore, if all of the receptors are free (i.e., $c(t) = 0$), we choose k_{a} so that Eq. 12 reduces to Eq. 7. In particular, we take

$$k_{\mathrm{a}} = \frac{\kappa D}{e_0 R} = 4D\varepsilon R\left(1 + \frac{4}{\varepsilon\pi\kappa_{\mathrm{rec}}}\right)^{-1} > 0. \tag{15}$$

Summarizing, the model consists of the following PDE with nonlinear coupling to an ODE through a boundary condition,

$$\begin{aligned}&\frac{\partial}{\partial t}u = D\Delta u, \quad r > R,\ t > 0,\\ &\lim_{r\to\infty} u(r,t) = u_0 > 0,\\ &D\frac{\partial}{\partial r}u(R,t) = k_{\mathrm{a}}(e_0 - c(t))u(R,t) - k_{\mathrm{b}}c(t),\\ &\frac{\mathrm{d}}{\mathrm{d}t}c(t) = k_{\mathrm{a}}(e_0 - c(t))u(R,t) - (k_{\mathrm{b}}+k_{\mathrm{c}})c(t).\end{aligned} \tag{16}$$

Michaelis-Menten boundary condition

Defining the dimensionless variables,

$$\bar{r} = \frac{r}{R}, \quad \bar{t} = \frac{t}{R^2/D}, \quad \bar{u} = \frac{u}{u_0}, \quad \bar{c} = \frac{c}{e_0},$$

Eq. 16 becomes

$$\begin{aligned}&\frac{\partial}{\partial \bar{t}}\bar{u} = \Delta\bar{u}, \quad \bar{r} > 1,\ \bar{t} > 0,\\ &\lim_{\bar{r}\to\infty}\bar{u}(\bar{r},\bar{t}) = 1,\\ &\frac{\partial}{\partial \bar{r}}\bar{u}(1,\bar{t}) = \kappa\big(1 - \bar{c}(\bar{t})\big)\bar{u}(1,\bar{t}) - \chi_{\mathrm{b}}\bar{c}(\bar{t}),\\ &\frac{\delta}{\kappa}\frac{\mathrm{d}}{\mathrm{d}\bar{t}}c(\bar{t}) = \bar{u}(1,\bar{t}) - \left(\frac{\chi_{\mathrm{b}}+\chi_{\mathrm{c}}}{\kappa} + \bar{u}(1,\bar{t})\right)\bar{c}(\bar{t}),\end{aligned} \tag{17}$$

where κ is in Eq. 8 and

$$\delta := \frac{N}{4\pi R^3}\frac{1}{u_0}, \quad \chi_{\mathrm{b}} := \frac{Nk_{\mathrm{b}}}{J_{\max}}, \quad \chi_{\mathrm{c}} := \frac{Nk_{\mathrm{c}}}{J_{\max}}. \tag{18}$$

Hence, the solution to Eq. 16 depends on the four dimensionless parameters, κ, δ, χ_{b}, and χ_{c}.

Notice that the parameter δ in Eq. 18 compares the volume concentrations of receptors to substrates. The Briggs-Haldane analysis of Michaelis-Menten enzyme kinetics assumes that this parameter is small (33). In particular, if

$$\delta \ll \kappa, \tag{19}$$

then we assume Eq. 17 is in quasi-steady state,

$$0 \approx \bar{u}(1,\bar{t}) - \left(\frac{\chi_{\mathrm{b}}+\chi_{\mathrm{c}}}{\kappa} + \bar{u}(1,\bar{t})\right)\bar{c}(\bar{t}),$$

and thus,

$$\bar{c}(\bar{t}) \approx \frac{\bar{u}(1,\bar{t})}{(\chi_{\mathrm{b}}+\chi_{\mathrm{c}})/\kappa + \bar{u}(1,\bar{t})}.$$

In this parameter regime, the problem in Eq. 16 becomes

$$\begin{aligned}&\frac{\partial}{\partial t}u = D\Delta u, \quad r > R,\ t > 0,\\ &\lim_{r\to\infty} u(r,t) = u_0 > 0,\\ &D\frac{\partial}{\partial r}u(R,t) = \frac{Vu(R,t)}{K + u(R,t)},\end{aligned} \tag{20}$$

where the maximal velocity and half-saturation constant in the boundary condition are

$$V := e_0k_{\mathrm{c}} = \frac{N}{4\pi R^2}k_{\mathrm{c}}, \quad K := \frac{k_{\mathrm{b}}+k_{\mathrm{c}}}{k_{\mathrm{a}}} = \frac{N(k_{\mathrm{b}}+k_{\mathrm{c}})}{4\pi DR\kappa}. \tag{21}$$

That is, the ODE boundary condition in Eq. 16 is replaced by a Michaelis-Menten type boundary condition in Eq. 20.

Steady-state uptake and receptor occupation

At steady state, solving the full PDE-ODE system in Eq. 16 is equivalent to solving the Michaelis-Menten system in Eq. 20. In either case, it is straightforward to obtain

$$\begin{aligned}u_{\mathrm{ss}}(r) &:= \lim_{t\to\infty}u(r,t) = u_0\left(1 - a\tfrac{R}{r}\right),\\ c_{\mathrm{ss}} &:= \lim_{t\to\infty}c(t) = \left(\tfrac{1-a}{(\chi_{\mathrm{b}}+\chi_{\mathrm{c}})/\kappa+1-a}\right)e_0,\end{aligned} \tag{22}$$

where a is the dimensionless parameter,

$$a = \frac{1}{2}\left(\chi_{\mathrm{c}} + \frac{\chi_{\mathrm{b}}+\chi_{\mathrm{c}}}{\kappa} + 1 - \sqrt{\left(\chi_{\mathrm{c}} + \frac{\chi_{\mathrm{b}}+\chi_{\mathrm{c}}}{\kappa} + 1\right)^2 - 4\chi_{\mathrm{c}}}\right). \tag{23}$$

The fraction of receptors that are bound at steady state is $c_{\mathrm{ss}}/e_0 \in (0, 1)$. The steady-state total flux into the cell is

$$J_* := D\int_{r=R}\frac{\mathrm{d}}{\mathrm{d}r}u_{\mathrm{ss}}\,\mathrm{d}S = aJ_{\max} < J_{\mathrm{bp}}. \tag{24}$$

The inequality in Eq. 24 is the desired result that the flux into the cell when the receptors have finite kinetics is strictly less than the flux into the cell when the receptors process molecules at infinite kinetic rates. To verify Eq. 24, note first that the case $\chi_{\mathrm{c}} = 0$ is trivial because $a = 0$ if and only if $\chi_{\mathrm{c}} = 0$. Next, suppose $\chi_{\mathrm{c}} > 0$. Note that Eq. 9 means $J_{\mathrm{bp}} = a_{\mathrm{bp}}J_{\max}$ where $a_{\mathrm{bp}} := \kappa/(\kappa+1)$. Hence, a_{bp} satisfies

$$a_{\mathrm{bp}} = \kappa\left(1 - a_{\mathrm{bp}}\right). \tag{25}$$

On the other hand, the boundary condition at $r = R$ implies that a satisfies

$$a = \frac{\kappa(1-a)}{1 + \chi_{\mathrm{b}}/\chi_{\mathrm{c}} + (\kappa/\chi_{\mathrm{c}})(1-a)}. \tag{26}$$

It is clear that the solution to Eq. 25 is larger than the solution to Eq. 26 because κ and χ_{c} are strictly positive. Therefore,

$$a \in \left(0, \frac{\kappa}{\kappa+1}\right) = \left(0, a_{\mathrm{bp}}\right),$$

which verifies Eq. 24.

In addition, fixing χ_{b} and κ and taking $\chi_{\mathrm{c}} \to \infty$ in Eq. 26 and comparing to Eq. 25 shows that

$$J_* = aJ_{\max} \to a_{\mathrm{bp}} J_{\max} = J_{\mathrm{bp}} \quad \text{as } \chi_{\mathrm{c}} \to \infty. \tag{27}$$

That is, J^* reduces to J_{bp} if the receptor turnover rate k_{c} is much faster than $J_{\max}/N$.

Other kinetic schemes and receptor internalization

The analysis above extends to more general kinetic schemes than the standard substrate-enzyme reaction in Eq. 11. Indeed, alternative kinetic schemes merely yield different systems of ODEs at the cell surface.

To illustrate, suppose that receptors transport substrate molecules by endocytosis (i.e., receptor internalization), which is often seen in eukaryotic cells (8–10). In this case, we replace Eq. 11 by

$$S + E \underset{k_{\mathrm{b}}}{\overset{k_{\mathrm{a}}}{\rightleftharpoons}} C \xrightarrow{k_{\mathrm{c}}} P, \quad E \xrightarrow{k_{\mathrm{c}}^0} \varnothing, \quad \varnothing \xrightarrow{k_{\mathrm{r}}} E,$$

where k_{c} and k_{c}^0 are the respective internalization rates for bound receptors C and free receptors E, and k_{r} is the rate that free receptors are delivered to the membrane. In this case, the boundary condition at $r = R$ in Eq. 12 for the substrate flux is unchanged and the ODEs in Eq. 13 become $\frac{\mathrm{d}}{\mathrm{d}t}e(t) = -k_{\mathrm{a}}e(t)u(R,t) + k_{\mathrm{b}}c(t) - k_{\mathrm{c}}^0 e(t) + k_{\mathrm{r}}$,

$$\frac{\mathrm{d}}{\mathrm{d}t}c(t) = k_{\mathrm{a}}e(t)u(R,t) - (k_{\mathrm{b}} + k_{\mathrm{c}})c(t).$$

Numerical methods and simulations

To verify the predictions of the modeling framework developed above, we perform numerical simulations of a stochastic, many-particle system. To reduce computational cost, the stochastic simulations are performed in a cylindrical spatial domain. We begin by extending the analysis above to this spatial domain.

Cylindrical domain

Let the spatial domain Ω be a cylinder of radius $2R_0 > 0$ and height $L > 0$,

$$\Omega := \left\{(x,y,z) \in \mathbb{R}^3 : x^2 + y^2 < 4R_0^2,\ z \in (0,L)\right\}. \tag{28}$$

Substrate molecules diffuse in Ω with reflecting boundaries at the top ($z = L$) and the sides ($r := \sqrt{x^2+y^2} = 2R_0$). Hence, the substrate concentration $u = u(x, y, z, t)$ satisfies

$$\frac{\partial}{\partial t}u = D\Delta u, \quad (x,y,z) \in \Omega,\ t > 0,$$

$$\frac{\partial}{\partial r}u = 0, \quad r = 2R_0; \qquad \frac{\partial}{\partial z}u = 0, \quad z = L.$$

Analogous to the surface of the sphere in the model above, we assume that the bottom of the cylinder ($z = 0$) is reflecting, except for $N >> 1$ small circular receptors.

If the receptors process substrates continuously, then the substrate concentration satisfies mixed boundary conditions at the bottom of the cylinder (analogous to Eq. 5),

$$D\frac{\partial}{\partial z}u = \frac{D}{R_0}\kappa_{\mathrm{rec}}u, \quad z = 0, \text{ and } (x,y) \text{ in a receptor},$$

$$\frac{\partial}{\partial z}u = 0, \quad z = 0, \text{ and } (x,y) \text{ not in a receptor}, \tag{29}$$

where κ_{rec} is as in Eq. 6. If the N receptors are roughly evenly distributed and have common radius $\varepsilon R_0 << R_0$, then Eq. 29 can be replaced by

$$D\frac{\partial}{\partial z}u = \frac{D}{R_0}\kappa u, \quad z = 0, \tag{30}$$

where κ is the same as in Eq. 8. Hence, the problem reduces to a one-dimensional PDE for $u = u(z, t)$,

$$\frac{\partial}{\partial t}u = D\Delta u, \quad z \in (0,L),\ t > 0 \tag{31}$$

and

$$\frac{\partial}{\partial z}u = 0, \quad z = L, \tag{32}$$

with the boundary condition in Eq. 30 at $z = 0$.

As above, we can incorporate finite receptor kinetics by replacing the boundary condition at $z = 0$ by a boundary condition that couples to an ODE. Specifically,

$$D\frac{\partial}{\partial z}u(0,t) = k_{\mathrm{a}}(e_0 - c(t))u(0,t) - k_{\mathrm{b}}c(t) \tag{33}$$

and

$$\frac{\mathrm{d}}{\mathrm{d}t}c(t) = k_{\mathrm{a}}(e_0 - c(t))u(0,t) - (k_{\mathrm{b}} + k_{\mathrm{c}})c(t), \tag{34}$$

where $c(t)$, e_0, k_{a}, k_{b}, and k_{c} are as above (with R replaced by R_0 in Eqs. 14 and 15). Furthermore, in the parameter regime in Eq. 19, we can eliminate Eq. 34 and replace Eq. 33 with a Michaelis-Menten type boundary condition with V and K given in Eq. 21,

$$D\frac{\partial}{\partial z}u(0,t) = \frac{Vu(0,t)}{K + u(0,t)}. \tag{35}$$

Stochastic simulation method

We now describe the stochastic simulation method. We use the standard Euler-Maruyama method (34) for simulating the paths of many diffusing substrate molecules in Ω with reflecting boundary conditions on the boundaries away from receptors. If a molecule hits a "free" receptor, then that molecule immediately binds to the receptor (corresponding to $\kappa_{\mathrm{rec}} = \infty$ in Eq. 6). If a receptor has a molecule bound to it, then that receptor is considered "occupied," and any other molecule that hits it simply reflects. We take $k_{\mathrm{b}} = 0$, and thus, a bound molecule is removed from the system after an exponentially distributed time with rate $k_{\mathrm{c}} > 0$. When a bound molecule is removed from the system, the corresponding receptor changes from "occupied" back to "free" and can thus bind additional molecules.

All stochastic simulations were written in a combination of C and MATLAB (The MathWorks, Natick, MA (35)). The simulations were completed in the cylinder in Eq. 28 with height $L = 1$ μm and radius $2R_0 = 0.1$ μm, with $N = 500$ receptors of common radius 0.001 μm placed uniformly at random (nonoverlapping) along the disk centered at $z = 0$. We take $D = 10^3$ $\mu\mathrm{m}^2$ s^{-1} and $k_{\mathrm{c}} \in \{10, 10^2, 10^3, 10^4\}$ s^{-1}.

Each trial began with all receptors "free" and 10^4 particles placed in the domain according to a normal distribution with mean $(x_0, y_0, z_0) = (0, 0, 0.9)$ μm and standard deviation 0.01 μm in each direction. For each value of k_c, 10 trials were completed with a discrete time step of 10^{-9} s. Additional trials and smaller time steps were tested on a subset of simulations and did not yield significant quantitative changes.

PDE numerical solution method

We numerically solve the PDE-ODE system (Eqs. 31, 32, 33, and 34) and the PDE with a Michaelis-Menten boundary condition (Eqs. 31, 32, and 35) with the method of lines (36). Essentially, this method approximates the PDE with a large system of ODEs by replacing spatial derivatives with finite differences. The method is fairly standard, but the nonstandard boundary conditions must be handled carefully.

We now give the details of the method. We approximate $u(z, t)$ at $n >> 1$ off-center grid points,

$$z_j := \left(j+\frac{1}{2}\right)\Delta z, \quad \text{for } j = 0, 1, \ldots, n-1, \tag{36}$$

where $\Delta z = L/n << L$, and denote the approximation by $u_j(t) \approx u(z_j, t)$. Replacing the Laplacian in Eq. 31 by a finite difference, $u_j(t)$ satisfies the ODE,

$$\frac{\mathrm{d}}{\mathrm{d}t}u_j = D\frac{(u_{j-1} - u_j + u_{j+1})}{(\Delta z)^2}, \text{ for } j = 0, 1, \ldots, n-1. \tag{37}$$

Notice that the equations for $\frac{\mathrm{d}}{\mathrm{d}t}u_0$ and $\frac{\mathrm{d}}{\mathrm{d}t}u_{n-1}$ in Eq. 37 involve u_{-1} and u_n, which are not yet defined. To ameliorate this issue, we make use of so-called ghost points, $z_{-1} := -\frac{1}{2}\Delta z$ and $z_n := \left(n+\frac{1}{2}\right)\Delta z$, and solve for u_{-1} and u_n using the boundary conditions. Specifically, we approximate the boundary condition at $z = L$ in Eq. 32 with a finite difference,

$$\frac{u_n - u_{n-1}}{\Delta z} = 0. \tag{38}$$

Hence, Eq. 38 implies $u_n = u_{n-1}$, which we then use to solve Eq. 37 when $j = n - 1$.

In the case of the PDE-ODE system, we approximate the boundary condition at $z = 0$ in Eq. 33 by

$$D\frac{(u_0 - u_{-1})}{\Delta z} = k_a(e_0 - c(t))\left(\frac{u_0 + u_{-1}}{2}\right) - k_b c(t), \tag{39}$$

where we have replaced $u(0, t)$ with $(u_0 + u_{-1})/2$. We then solve Eq. 39 for u_{-1} and use this in Eq. 37 when $j = 0$. In addition to the n ODEs in Eq. 37, we also have the ODE for $c(t)$, which is obtained from Eq. 34 upon replacing $u(0, t)$ by $(u_0 + u_{-1})/2$.

In the case of the Michaelis-Menten boundary condition, we approximate Eq. 35 by

$$D\frac{(u_0 - u_{-1})}{\Delta z} = \frac{V(u_0 + u_{-1})/2}{K + (u_0 + u_{-1})/2}. \tag{40}$$

We then solve Eq. 40 for $u_{-1} > 0$ and use this in Eq. 37 when $j = 0$.

Summarizing, the PDE-ODE system is approximated by $n + 1$ ODEs, and the PDE with a Michaelis-Menten boundary condition is approximated by n ODEs. In either case, the ODEs are solved using the ode15s function in MATLAB (35) with $n = 10^3$ spatial grid points.

Code availability

Code for reproducing the stochastic and PDE numerical simulations is available on the GitHub database (https://github.com/gregoryhandy).

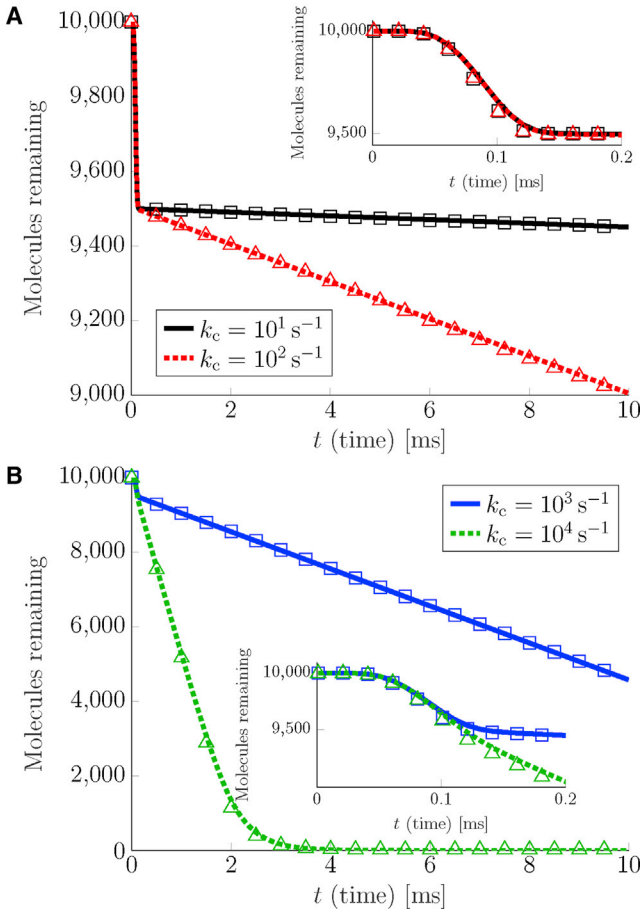

FIGURE 2 Comparison of stochastic simulations (*squares and triangles*) to the deterministic PDE-ODE system (*solid and dotted curves*) for the cylindrical domain for different values of the receptor turnover rate k_c. The insets zoom in at early times. See the text for details. To see this figure in color, go online.

RESULTS AND DISCUSSION

Analysis confirmed by stochastic simulations

In Fig. 2, we plot the results of stochastic simulations (*squares* and *triangles*) and the solution to the deterministic PDE-ODE system (*solid* and *dotted curves*) for the cylindrical spatial domain in Eq. 28 for various choices of the receptor turnover rate k_c. Specifically, we plot the number of diffusing molecules remaining in the domain (molecules which are unbound and have not been absorbed) as a function of time. This plot shows that the PDE-ODE system accurately describes the dynamics of the full stochastic system involving many interacting particles.

Notice in Fig. 2 that at early times ($t < 0.2$ ms), the number of remaining molecules rapidly drops from 10,000 to 9500, which corresponds to 500 molecules quickly binding the $N = 500$ receptors. This initial rapid decrease is seen in both the PDE-ODE solution and the stochastic simulations, which is evident from the insets in Fig. 2, which zoom in at early times. Then as time increases, the number of

remaining molecules decreases linearly with a slope of Nk_c, which is readily seen in Fig. 2 for both the PDE-ODE solution and the stochastic simulations.

The PDE solution with a Michaelis-Menten boundary condition also produces the desired linear decay with slope Nk_c, but it does not exhibit the initial rapid decay of N molecules binding to the N receptors (plot not shown). This is not surprising because the Michaelis-Menten boundary condition was derived assuming that there are many more diffusing molecules than receptors per some characteristic volume. Indeed, in such a parameter regime, the size of the initial drop in the number of molecules (namely the number of receptors, N) would be small compared to the number of molecules and would thus be negligible.

To reduce computational expense, the simulations were performed in a bounded, cylindrical spatial domain rather the unbounded domain exterior to a sphere in Eq. 3. However, we expect that the agreement between stochastic simulations and the PDE-ODE framework seen here extends to more general geometries, including the unbounded spherical geometry of Eq. 3. In fact, the cylindrical domain in Eq. 28 can model a cylindrical region of height $L = 1\ \mu$m and radius $2R_0 = 0.1\ \mu$m directly above a cell, where the base of the cylinder represents a flat patch of cell membrane with many receptors. In particular, for cells of radius $R \geq 1\mu$m, the membrane curvature is negligible at the base of a cylinder of radius $2R_0 = 0.1\ \mu$m.

Parameter ranges

Before discussing some biophysical implications of our analysis, we briefly discuss parameter values. We do not seek precise values for any one specific application, but rather, we choose ranges and orders of magnitude that are relevant across multiple systems. Unless otherwise noted, the following "default" parameter values are used in the figures and calculations below. The parameters are summarized in Table 1.

Cell radii range from roughly 0.35 μm for a small bacterium to 15 μm for a large mammalian cell (31). We set the default radius to be $R = 1\ \mu$m, which is consistent with a bacterial cell or a small eukaryotic cell. We set the default diffusion coefficient to be $D = 10^3\ \mu\text{m}^2\ \text{s}^{-1}$, which is the order of magnitude relevant for glucose uptake by an *Escherichia coli* cell or a yeast cell (37–40) and chemotaxis by bacterial cells and slime mold (2). Following (2,27), we take the radius of each receptor to be $\varepsilon R = 1$ nm and $\kappa_{\text{rec}} = \infty$, which means $\varepsilon = 10^{-3}$ and $\kappa = \varepsilon N/\pi$. The number of receptors N on a cell can vary greatly (4,41,42), and we take $N = 10^3$ as the default value. Extracellular concentrations of interest also vary considerably. For example, a characteristic value in (2) is $u_0 = 1\ \mu$M, the nutrient uptake study (27) considers $u_0 = 100\ \mu$M, and other nutrient uptake studies involve u_0 on the order of $10^3\ \mu$M or greater (37,38,40). We follow (2) and take $u_0 = 1\ \mu$M as the default value.

Finally, the kinetic rate parameters k_b and k_c can also vary considerably. The typical turnover rate for sugar transporters is $k_c = 10^2\ \text{s}^{-1}$, with a range of $k_c \in [3 \times 10^1\ \text{s}^{-1}, 3 \times 10^2\ \text{s}^{-1}]$, though chloride-bicarbonate transporters can reach speeds on the order of $k_c = 10^5\ \text{s}^{-1}$ (31). We take $k_c = 10^2\ \text{s}^{-1}$ as the default value. Breakup rates k_b have been estimated on the order of $10^{-4}\ \text{s}^{-1}$ (8), $10^{-3}\ \text{s}^{-1}$ (8,43), $1\ \text{s}^{-1}$ (43), and $10^4\ \text{s}^{-1}$ (2). Because most values satisfy $k_b << k_c$, we take $k_b = 0$ as the default value for simplicity.

TABLE 1 Summary of parameter values and ranges

Parameter	Default value	Range of interest
D (molecule diffusivity)	$10^3\ \mu\text{m}^2\ \text{s}^{-1}$	$[10^2, 10^3]\ \mu\text{m}^2\ \text{s}^{-1}$
R (cell radius)	$1\ \mu$m	[0.35, 15] μm
ε (receptor/cell radius ratio)	10^{-3}	
N (number of receptors)	10^3	$[10^2, 10^5]$
κ_{rec} (receptor trapping rate)	∞	
u_0 (extracellular concentration)	$1\ \mu$M	[1 nM, 1 mM]
k_c (receptor turnover rate)	$10^2\ \text{s}^{-1}$	$[10^1, 10^5]\ \text{s}^{-1}$
k_b (receptor unbinding rate)	0	$[0, 10^4]\ \text{s}^{-1}$

Unless otherwise noted, the "default" values are used in the figures and calculations. See the text for details.

Receptor kinetics can dominate uptake

In this subsection, we use our uptake formula (J^* in Eqs. 23 and 24) to show that finite receptor kinetics play a dominant role in cellular uptake in some typical biophysical scenarios. In Fig. 3 *a*, we plot the ratio $J^*/J_{\max}$ as a function of the number of receptors N for different values of the receptor turnover rate k_c. Note that J^* reduces to the Berg-Purcell flux, J_{bp}, if k_c is infinite (see Eq. 27). This figure shows that J^* is much less than J_{bp} for typical values of the receptor turnover rate k_c. For example, if $k_c = 10^2\ \text{s}^{-1}$ and the rest of the parameters are the default values in Table 1, then

$$\frac{J_*}{J_{\text{bp}}} \approx 0.05. \tag{41}$$

The reason for the significant discrepancy in Eq. 41 is that a large fraction of molecules that hit a receptor are blocked from binding because that receptor is occupied by another molecule (this is incorporated into J^* but ignored by J_{bp}). Indeed, at these default parameter values, Eq. 22 implies that more than 95% of the surface receptors are bound to a molecule at any given time. Hence, any molecule that manages to hit a receptor has less than a 5% chance of binding upon first contact with that receptor.

It is also evident from Fig. 3 *a* that J_{bp} saturates at much smaller values of N compared with J^*. For example, increasing the receptor number from $N = 10^4$ to $N = 10^5$ increases J_{bp} by a mere 27%, whereas this increase in the receptor number increases J^* by more than 600% if $k_c = 10^2\ \text{s}^{-1}$.

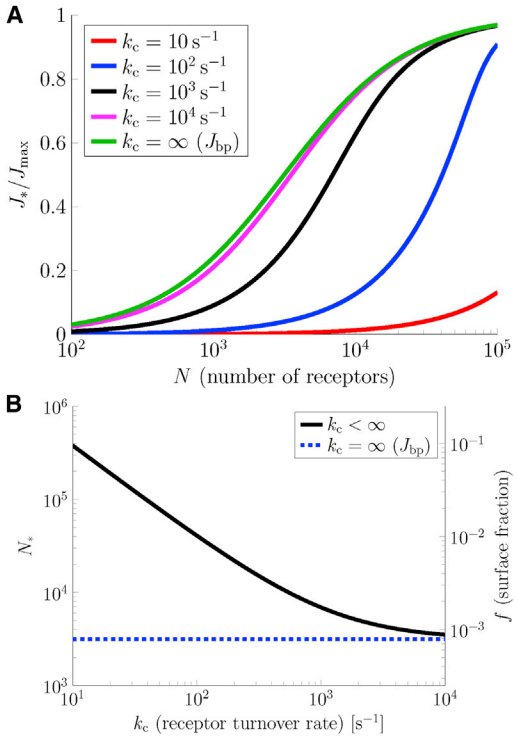

FIGURE 3 (*a*) Cellular uptake as a function of the number of cell surface receptors for different turnover rates k_c. (*b*) Number of receptors needed so that $J^* = J_{bp}$ (N^* in Eq. 42) on the left axis as a function of k_c. The right axis gives the corresponding fraction of the cell surface covered by receptors (f in Eq. 44). See Table 1 for parameter values. To see this figure in color, go online.

This is because in the calculation of J_{bp}, increasing the number of receptors merely increases the likelihood that a single molecule hits a receptor rather than escaping to spatial infinity. In contrast, if we include finite receptor kinetics, then increasing the number of receptors also increases the number of molecules that can be bound to the cell at any one time.

To further investigate this point, in Fig. 3 *b* we plot on the left axis the number of receptors, N^*, required for J^* to reach one-half of J_{max} as a function of k_c. That is, we plot

$$N_* := \frac{\pi}{\varepsilon} + \frac{J_{max}}{2k_c} + \frac{\pi k_b}{k_c}, \tag{42}$$

where the formula in Eq. 42 was found by setting $J^* = J_{max}/2$ and solving for N. The corresponding number of receptors required for the Berg-Purcell flux, J_{bp}, to reach $J_{max}/2$ is

$$\lim_{k_c \to \infty} N_* = \tfrac{\pi}{\varepsilon}. \tag{43}$$

Using Eqs. 42 and 43, we see that J_{bp} reaches one-half of J_{max} with $N^* \approx 3 \times 10^3$ receptors ($k_c = \infty$), whereas J^* requires $N^* \approx 4 \times 10^4$ receptors to reach one-half of J_{max} if $k_c = 10^2\ s^{-1}$.

On the right axis of Fig. 3 *b*, we plot the corresponding fraction of the cell surface covered by receptors,

$$f := \frac{\pi(\varepsilon R)^2 N_*}{4\pi R^2} = \frac{\varepsilon^2 N_*}{4} \in (0,1). \tag{44}$$

Interestingly, f is very small as long as k_c is not very slow. For example, $f \approx 10^{-3} = 0.1\%$ for $N^* = 3 \times 10^3$, and $f = 10^{-2} = 1\%$ for $N^* = 4 \times 10^4$. Therefore, the remarkable result of Berg and Purcell that a cell requires only a small receptor surface fraction f to have uptake near the maximal J_{max} still holds in the case of finite receptor kinetics.

As mentioned in the Introduction, many previous works have sought to modify and refine the Berg-Purcell formula to incorporate various details in the problem (16–26). It is therefore worth pointing out that the discrepancy between J^* and J_{bp} is much greater than some previous modifications of J_{bp}. For example, Zwanzig posited the formula (15)

$$J_{zw} := \frac{\varepsilon N}{\varepsilon N + (1 - \varepsilon^2 N/4)\pi} J_{max}$$

to account for the effects of interference between receptors. However, the percentage difference between J_{bp} and J_{zw} is less than the dimensionless receptor radius ε (25),

$$\frac{J_{zw} - J_{bp}}{J_{zw}} = \frac{N\pi\varepsilon^2}{4N\varepsilon + 4\pi} \le \lim_{N \to \infty} \frac{N\pi\varepsilon^2}{4N\varepsilon + 4\pi} \le \varepsilon \tfrac{\pi}{4} < \varepsilon.$$

That is, J_{zw} and J_{bp} typically differ by around one tenth of one percent, whereas J^* and J_{bp} can differ by at least an order of magnitude in typical biophysical scenarios.

Uptake is almost Michaelis-Menten

The discrepancy between J^* and J_{bp} vanishes at low extracellular concentrations and is magnified at high extracellular concentrations. In Fig. 4, we plot J^* and J_{bp} as functions of the extracellular concentration u_0. Here, we see that J^* and J_{bp} are indistinguishable at low concentrations (even for slow k_c-values), whereas J^* can be several orders of magnitude less than J_{bp} at high concentrations. The explanation for this is straightforward. At sufficiently low concentrations, molecules arrive at receptors at a much slower rate

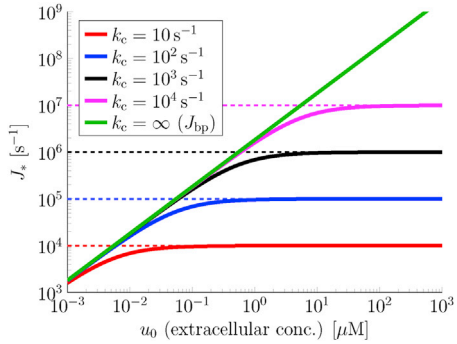

FIGURE 4 Cellular uptake as a function of the extracellular concentration for different turnover rates k_c. The dashed horizontal lines are the maximal uptake rates for different turnover rates. See Table 1 for parameter values. To see this figure in color, go online.

than receptors can process molecules, which is the assumption used to derive J_{bp} (2). Because the per receptor arrival rate is J_{bp}/N and the receptor kinetic rates are k_{b} and k_{c}, a sufficiently low concentration is defined by the following dimensionless number being much less than one,

$$\rho : = \frac{J_{\mathrm{bp}}/N}{k_{\mathrm{b}} + k_{\mathrm{c}}} = \frac{\frac{\kappa}{\kappa+1} 4\pi D R u_0}{N(k_{\mathrm{b}} + k_{\mathrm{c}})} \ll 1. \tag{45}$$

As the concentration increases and Eq. 45 is violated, the arrival rate exceeds the receptor kinetic rates, and thus, receptor kinetics modify cellular uptake.

It is intuitively clear that cellular uptake cannot increase linearly as a function of u_0 indefinitely, but rather, uptake must saturate at some maximal rate. In light of this observation, a Michaelis-Menten functional form for the uptake rate is often posited (6),

$$J_{\mathrm{mm}} : = \frac{V_{\max} u_0}{K_{\mathrm{M}} + u_0}, \tag{46}$$

for some maximal uptake rate $V_{\max}$ and half-saturation constant K_{M}. We stress that the uptake equation in Eq. 46 is not to be confused with the boundary condition in Eq. 20, which was derived to approximate the PDE-ODE system in Eq. 16.

The values of $V_{\max}$ and K_{M} in Eq. 46 are usually determined by matching Eq. 46 to experimental data. However, it is possible to relate $V_{\max}$ and K_{M} to microscopic biophysical parameters. First, it is clear that the maximal uptake rate must be $V_{\max} = Nk_{\mathrm{c}}$. Next, if we force J_{mm} to coincide with J_{bp} at low concentrations (i.e., $u_0 << K_{\mathrm{M}}$), then we must have

$$K_{\mathrm{M}} = \frac{V_{\max} u_0}{J_{\mathrm{bp}}} = \frac{Nk_{\mathrm{c}}(1+\kappa)}{4\pi D R \kappa}. \tag{47}$$

Now, it is straightforward to use Eqs. 23 and 24 to check that J^* has the desired property that it saturates at Nk_{c} at high concentrations,

$$\lim_{u_0 \to \infty} J_* = Nk_{\mathrm{c}},$$

and J^* reduces to J_{bp} at low concentrations,

$$\lim_{u_0 \to 0} J_* \Big/ J_{\mathrm{bp}} = 1.$$

Hence, J^* and J_{mm} agree at high and low concentrations. However, it is evident from the formula for J^* in Eqs. 23 and 24 that $J^* \neq J_{\mathrm{mm}}$ at intermediate concentrations.

In Fig. 5 *a*, we plot J^* (*solid curves*) and J_{mm} (*dotted curves*) as functions of the concentration for $k_{\mathrm{b}} = 0$. Although J^* does not have the exact Michaelis-Menten functional form as in Eq. 46, this plot shows that the J^* curve does have a profile very similar to the profile generated by the Michaelis-Menten functional form (i.e., a sigmoidal curve). This is an important feature of the formula for J^*, as this profile is observed in experiments measuring cellular uptake (6,37–39).

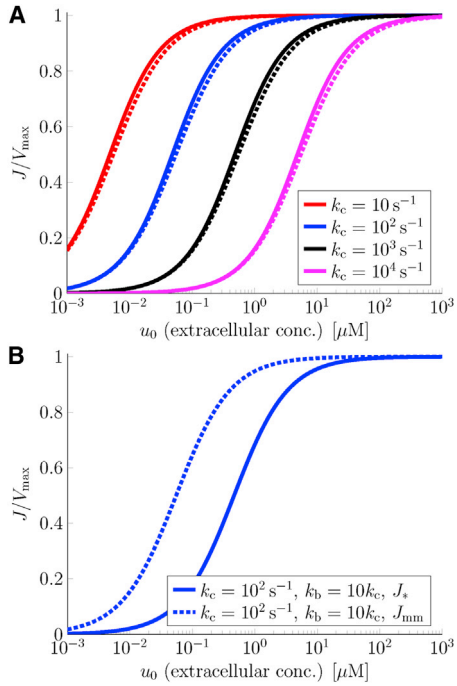

FIGURE 5 Cellular uptake as a function of the extracellular concentration for different turnover rates k_{c}, with breakup rate $k_{\mathrm{b}} = 0$ in (*a*) and $k_{\mathrm{b}} = 10k_{\mathrm{c}}$ in (*b*). The solid curves correspond to J^* in Eqs. 23 and 24, and the dotted curves correspond to J_{mm} in Eq. 46. See Table 1 for other parameter values. To see this figure in color, go online.

Furthermore, it is straightforward to use the formula in Eqs. 23 and 24 for J^* to find the half-saturation constant (i.e., the "apparent K_{M}" of J^*). Indeed, solving the equation $J^* = V_{\max}/2$ for the concentration u_0 gives the half-saturation constant,

$$K_{\mathrm{M}}^* : = \frac{Nk_{\mathrm{c}}(1+\kappa/2)}{4\pi D R \kappa} + \frac{Nk_{\mathrm{b}}}{4\pi D R \kappa}. \tag{48}$$

Comparing Eq. 48 with Eq. 47, we see that these two half-saturation constants are similar if $k_{\mathrm{b}} << k_{\mathrm{c}}$. Indeed, the close agreement between J^* and J_{mm} in Fig. 5 *a* results from taking $k_{\mathrm{b}} = 0$. However, it follows from comparing Eqs. 48 and 47 that taking k_{b} not much less than k_{c} can make J_{mm} saturate at much lower concentrations than J^*. This is illustrated in Fig. 5 *b*, in which we plot J^* and J_{mm} with $k_{\mathrm{b}} = 10k_{\mathrm{c}}$.

CONCLUSIONS

We have developed a framework for modeling molecular species that diffuse in a three-dimensional bulk region and interact with receptors embedded on a two-dimensional surface. The receptors bind and process molecules at finite kinetic rates, which introduces significant statistical correlations between the individual diffusing molecules. We developed the framework in the context of the Berg-Purcell cellular uptake model (2). We found that in some typical

biophysical scenarios of interest, finite receptor kinetics can reduce cellular uptake by at least an order of magnitude compared with the Berg-Purcell estimate. The predictions of our analysis were confirmed by numerical simulations of a many-particle stochastic system.

Mathematically, the framework uses the theory of boundary homogenization to couple a PDE (the diffusion equation) to nonlinear ODEs on a boundary. In a certain parameter regime (or at steady state), the boundary conditions can be reduced to a nonlinear, Michaelis-Menten flux condition. Several interesting prior works have used PDEs with ODE boundary conditions to model reaction-diffusion systems (44–50). These prior works have generally studied Turing patterns and spatiotemporal oscillations. To estimate how receptor diffusion and cellular rotation influence cellular uptake, (25) used the diffusion equation with boundary conditions described by stochastic differential equations.

In contrast to both this work and (44–50), some models have coupled bulk diffusion to surface reactions by analyzing the concentration in a thin layer near the surface (51–54). For example, the ODE in Eq. 4 in (53) describes the time evolution of the volume concentration of unbound molecules in a thin layer of width $l > 0$ of the surface, where the width of the layer can be derived from the potential mean force near the boundary. Here, we implicitly assume a flat potential, allowing us to set $l = 0$. Setting $l = 0$ in Eq. 4 in (53) yields Eq. 12 in this work, where F and $q_1\Gamma_1$ in (53) correspond to $k_a e(t)u(R, t)$ and $k_b c(t)$, respectively, in this work. Although our simulations and theory can be extended to account for $l > 0$, Fig. 4 in (53) suggests the results will only differ at very short times, leaving our results regarding the steady-state flux unchanged.

Following Berg and Purcell (2), a series of works have studied the ability of a cell to estimate an external concentration based on receptor occupancy (8,55–60). Such estimates are inherently noisy because they depend on the stochastic diffusion, binding, and unbinding of single molecules. To approximate the accuracy of cell sensing over a finite time period, these works often estimate the variance in receptor occupancy. Many prior models consider only a single receptor, and there have been conflicting results even in this simplified scenario (59). (57) considered a cell with a finite set of receptors that bind and unbind molecules according to a continuous-time Markov chain with rate constants that depend on the diffusion coefficient. In our model, we have taken a continuum limit of receptors and consider concentrations of free and bound receptors. Although our approach provides analytical results pertaining to the steady-state flux, it does not yield results pertaining to the variance in receptor occupancy.

Previous works have employed mathematical models to study how finite receptor kinetics affect diffusive uptake. (11,12) formulated and analyzed stochastic models of diffusive interactions with receptors that must wait a transitory "recharge" time between captures. In (11), it was proven that such a recharge time can drastically reduce the number of captured molecules (the number of captures grows logarithmically in the number of total molecules versus linear growth in the absence of recharge). (12) used a variety of stochastic models to analyze similar systems. There is a rather large amount of literature on cellular nutrient uptake that takes the Michaelis-Menten uptake equation in Eq. 46 as its starting point (6,37–39). The maximal uptake rate and half-saturation constant (i.e., $V_{\max}$ and K_M) are chosen to fit experimental uptake rates. Our uptake formula (J^* in Eqs. 23 and 24) does not have the Michaelis-Menten functional form in Eq. 46, but it nevertheless exhibits the same sigmoidal uptake curve as a function of the extracellular concentration.

Although we developed the framework in the context of cellular uptake in a spherical geometry, it can be applied to other systems with potentially different geometries and receptor kinetic schemes. For example, synaptic transmission involves neurotransmitter molecules diffusing across the synaptic cleft and binding to receptors on the adjacent neuron (5). In this case, the shape of the synaptic cleft is similar to a cylinder, and the framework of our study could be used to investigate the effect of the finite kinetic rates of neural receptors. As another example amenable to this framework, cylindrical domains with receptors on the "sides" have been used to model catheter-based drug delivery systems (61).

Finally, we conclude by discussing the important study by Wagner et al. (27) on nutrient uptake by bacterial cells. This work used fluorescent tracing to show that bacterial cell "stalks," which are long and thin extensions of the cell envelope, can bind and import nutrients from the extracellular environment. These authors then used novel mathematical analysis to generalize the Berg-Purcell model to a domain exterior to a stalk (modeled by a prolate spheroid). Based on this analysis, the authors argued that the stalk morphology increases nutrient uptake compared to a sphere. For future work, it would be interesting to extend the analysis in this work to the geometry considered in (27) to investigate the effect of finite receptor kinetics.

Indeed, the model in (27) assumes that receptors can absorb nutrient molecules continuously. As in Berg-Purcell, this assumption is valid if receptors can import molecules at a much faster rate than molecules tend to arrive at receptors. We now use the parameter ρ in Eq. 45 to compare these two rates in (27), where $\rho << 1$ means that receptor kinetics are much faster than arrivals. The model in (27) considered $N = 10^4$ perfectly absorbing receptors (meaning $\kappa_{rec} = \infty$ in our notation). The radius of each receptor was 1 nm, and stalk lengths varied from 1 to 10 μm. The extracellular concentration used in the experiments was $u_0 = 100$ μM. If we take these values and set $R = 1$ μm, $D = 10^3$ $\mu m^2\ s^{-1}$, and

$k_b = 0$ in Eq. 45, then the receptor turnover rate k_c would need to satisfy

$$k_c \gg 5.7 \times 10^4 \text{ s}^{-1}$$

to have $\rho << 1$. That is, a single receptor would need to import molecules at a rate much faster than 10^4 s^{-1}, whereas characteristic rates are on the order of 10^2 s^{-1} (31). Although this simple calculation ignores the stalk geometry, it nevertheless suggests that finite receptor kinetics may play an important role in the uptake rate for the system studied in (27). More broadly, the framework developed in this study provides a method for investigating how receptor kinetics affect a variety of biophysical systems.

ACKNOWLEDGMENTS

G.H. was supported by The Swartz Foundation. S.D.L. was supported by the National Science Foundation (grant numbers DMS-1944574, DMS-1814832, and DMS-1148230).

REFERENCES

1. Johnston, M. 1999. Feasting, fasting and fermenting. Glucose sensing in yeast and other cells. *Trends Genet.* 15:29–33.
2. Berg, H. C., and E. M. Purcell. 1977. Physics of chemoreception. *Biophys. J.* 20:193–219.
3. Sela-Culang, I., V. Kunik, and Y. Ofran. 2013. The structural basis of antibody-antigen recognition. *Front. Immunol.* 4:302.
4. Perelson, A. S., and G. Weisbuch. 1997. Immunology for physicists. *Rev. Mod. Phys.* 69:1219–1268.
5. Deutch, A. 2013. Chapter 6. *In* Fundamental Neuroscience, Fourth Edition. Elsevier, pp. 117–138.
6. Fiksen, Ø., M. J. Follows, and D. L. Aksnes. 2013. Trait-based models of nutrient uptake in microbes extend the Michaelis-Menten framework. *Limnol. Oceanogr.* 58:193–202.
7. Aksnes, D. L., and F. J. Cao. 2011. Inherent and apparent traits in microbial nutrient uptake. *Mar. Ecol. Prog. Ser.* 440:41–51.
8. Aquino, G., and R. G. Endres. 2010. Increased accuracy of ligand sensing by receptor internalization. *Phys. Rev. E Stat. Nonlin. Soft Matter Phys.* 81:021909.
9. Ferguson, S. S. 2001. Evolving concepts in G protein-coupled receptor endocytosis: the role in receptor desensitization and signaling. *Pharmacol. Rev.* 53:1–24.
10. Mukherjee, S., R. N. Ghosh, and F. R. Maxfield. 1997. Endocytosis. *Physiol. Rev.* 77:759–803.
11. Handy, G., S. D. Lawley, and A. Borisyuk. 2018. Receptor recharge time drastically reduces the number of captured particles. *PLoS Comput. Biol.* 14:e1006015.
12. Handy, G., S. D. Lawley, and A. Borisyuk. 2019. Role of trap recharge time on the statistics of captured particles. *Phys. Rev. E.* 99:022420.
13. Handy, G., M. Taheri, …, A. Borisyuk. 2017. Mathematical investigation of IP_3-dependent calcium dynamics in astrocytes. *J. Comput. Neurosci.* 42:257–273.
14. Smoluchowski, M. 1917. Grundriss der Koagulationskinetik kolloider Lösungen. *Kolloid-Zeitschrift.* 21:98–104.
15. Zwanzig, R. 1990. Diffusion-controlled ligand binding to spheres partially covered by receptors: an effective medium treatment. *Proc. Natl. Acad. Sci. USA.* 87:5856–5857.
16. Zwanzig, R., and A. Szabo. 1991. Time dependent rate of diffusion-influenced ligand binding to receptors on cell surfaces. *Biophys. J.* 60:671–678.
17. Bernoff, A. J., A. E. Lindsay, and D. D. Schmidt. 2018. Boundary homogenization and capture time distributions of semipermeable membranes with periodic patterns of reactive sites. *Multiscale Model. Simul.* 16:1411–1447.
18. Lindsay, A. E., A. J. Bernoff, and M. J. Ward. 2017. First passage statistics for the capture of a brownian particle by a structured spherical target with multiple surface traps. *Multiscale Model. Simul.* 15:74–109.
19. Berezhkovskii, A. M., Y. A. Makhnovskii, …, S. Y. Shvartsman. 2004. Boundary homogenization for trapping by patchy surfaces. *J. Chem. Phys.* 121:11390–11394.
20. Berezhkovskii, A. M., M. I. Monine, …, S. Y. Shvartsman. 2006. Homogenization of boundary conditions for surfaces with regular arrays of traps. *J. Chem. Phys.* 124:036103.
21. Dagdug, L., M. V. Vázquez, …, V. Y. Zitserman. 2016. Boundary homogenization for a sphere with an absorbing cap of arbitrary size. *J. Chem. Phys.* 145:214101.
22. Eun, C. 2017. Effect of surface curvature on diffusion-limited reactions on a curved surface. *J. Chem. Phys.* 147:184112.
23. Muratov, C. B., and S. Y. Shvartsman. 2008. Boundary homogenization for periodic arrays of absorbers. *Multiscale Model. Simul.* 7:44–61.
24. Eun, C. 2020. Effects of the size, the number, and the spatial arrangement of reactive patches on a sphere on diffusion-limited reaction kinetics: a comprehensive study. *Int. J. Mol. Sci.* 21:997.
25. Lawley, S. D., and C. E. Miles. 2019. How receptor surface diffusion and cell rotation increase association rates. *SIAM J. Appl. Math.* 79:1124–1146.
26. Kaye, J., and L. Greengard. 2020. A fast solver for the narrow capture and narrow escape problems in the sphere. *J. Comput. Phys. X.* 5:100047, Published online December 12, 2019.
27. Wagner, J. K., S. Setayeshgar, …, Y. V. Brun. 2006. A nutrient uptake role for bacterial cell envelope extensions. *Proc. Natl. Acad. Sci. USA.* 103:11772–11777.
28. Shoup, D., and A. Szabo. 1982. Role of diffusion in ligand binding to macromolecules and cell-bound receptors. *Biophys. J.* 40:33–39.
29. Lawley, S. D. 2019. Boundary homogenization for trapping patchy particles. *Phys. Rev. E.* 100:032601.
30. Plunkett, C. E., and S. D. Lawley. 2021. Bimolecular binding rates for pairs of spherical molecules with small binding sites. *Multiscale Model. Simul.* 19:148–183.
31. Milo, R., P. Jorgensen, …, M. Springer. 2010. BioNumbers–the database of key numbers in molecular and cell biology. *Nucleic Acids Res.* 38:D750–D753.
32. Gunawardena, J. 2007. Distributivity and processivity in multisite phosphorylation can be distinguished through steady-state invariants. *Biophys. J.* 93:3828–3834.
33. Keener, J. P., and J. Sneyd. 2010. Mathematical Physiology: I: Cellular Physiology. Springer-Verlag, New York.
34. Kloeden, P. E., and E. Platen. 1992. Numerical Solution of Stochastic Differential Equations. Springer, Berlin.
35. The MathWorks Inc. 2019. MATLAB R2019a version 9.6. The MathWorks Inc., Natick, MA.
36. LeVeque, R. J. 2007. Finite Difference Methods for Ordinary and Partial Differential Equations: Steady-State and Time-Dependent Problems. SIAM, Philadelphia, PA.
37. Meijer, M. M., J. Boonstra, …, C. T. Verrips. 1996. Kinetic analysis of hexose uptake in *Saccharomyces cerevisiae* cultivated in continuous culture. *Biochim. Biophys. Acta.* 1277:209–216.
38. Maier, A., B. Völker, …, G. F. Fuhrmann. 2002. Characterisation of glucose transport in *Saccharomyces cerevisiae* with plasma membrane vesicles (countertransport) and intact cells (initial uptake) with single Hxt1, Hxt2, Hxt3, Hxt4, Hxt6, Hxt7 or Gal2 transporters. *FEMS Yeast Res.* 2:539–550.

39. Natarajan, A., and F. Srienc. 1999. Dynamics of glucose uptake by single *Escherichia coli* cells. *Metab. Eng.* 1:320–333.

40. Lavrentovich, M. O., J. H. Koschwanez, and D. R. Nelson. 2013. Nutrient shielding in clusters of cells. *Phys. Rev. E Stat. Nonlin. Soft Matter Phys.* 87:062703.

41. Ismael, A., W. Tian, …, D. E. Stone. 2016. Gβ promotes pheromone receptor polarization and yeast chemotropism by inhibiting receptor phosphorylation. *Sci. Signal.* 9:ra38.

42. Lawley, S. D., A. E. Lindsay, and C. E. Miles. 2020. Receptor organization determines the limits of single-cell source location detection. *Phys. Rev. Lett.* 125:018102.

43. Mugler, A., A. Levchenko, and I. Nemenman. 2016. Limits to the precision of gradient sensing with spatial communication and temporal integration. *Proc. Natl. Acad. Sci. USA.* 113:E689–E695.

44. Levine, H., and W.-J. Rappel. 2005. Membrane-bound Turing patterns. *Phys. Rev. E Stat. Nonlin. Soft Matter Phys.* 72:061912.

45. Gomez-Marin, A., J. Garcia-Ojalvo, and J. M. Sancho. 2007. Self-sustained spatiotemporal oscillations induced by membrane-bulk coupling. *Phys. Rev. Lett.* 98:168303.

46. Gou, J., and M. Ward. 2016. An asymptotic analysis of a 2- model of dynamically active compartments coupled by bulk diffusion. *J. Nonlinear Sci.* 26:979–1029.

47. Gou, J., W.-Y. Chiang, …, Y.-X. Li. 2017. A theory of synchrony by coupling through a diffusive chemical signal. *Physica D. Nonlinear Phenomena.* 339:1–17.

48. Gomez, D., M. J. Ward, and J. Wei. 2019. The linear stability of symmetric spike patterns for a bulk-membrane coupled Gierer–Meinhardt model. *SIAM J. Appl. Dyn. Syst.* 18:729–768.

49. David, J. F., S. A. Iyaniwura, …, F. Brauer. 2020. A novel approach to modelling the spatial spread of airborne diseases: an epidemic model with indirect transmission. *Math. Biosci. Eng.* 17:3294–3328.

50. Bressloff, P. C., and S. D. Lawley. 2017. Dynamically active compartments coupled by a stochastically-gated gap junction. *J. Nonlinear Sci.* 27:1487–1512.

51. Ward, A. F. H., and L. Tordai. 1946. Time-dependence of boundary tensions of solutions I. The role of diffusion in time-effects. *J. Chem. Phys.* 14:453–461.

52. Diamant, H., G. Ariel, and D. Andelman. 2001. Kinetics of surfactant adsorption: the free energy approach. *Colloids Surf. A Physicochem. Eng. Asp.* 183–185:259–276.

53. Chou, T., and M. R. D'Orsogna. 2007. Multistage adsorption of diffusing macromolecules and viruses. *J. Chem. Phys.* 127:105101.

54. Fok, P.-W., and T. Chou. 2009. Interface growth driven by surface kinetics and convection. *SIAM J. Appl. Math.* 70:24–39.

55. Bialek, W., and S. Setayeshgar. 2005. Physical limits to biochemical signaling. *Proc. Natl. Acad. Sci. USA.* 102:10040–10045.

56. Endres, R. G., and N. S. Wingreen. 2009. Maximum likelihood and the single receptor. *Phys. Rev. Lett.* 103:158101.

57. Berezhkovskii, A. M., and A. Szabo. 2013. Effect of ligand diffusion on occupancy fluctuations of cell-surface receptors. *J. Chem. Phys.* 139:121910.

58. Kaizu, K., W. de Ronde, …, P. R. ten Wolde. 2014. The Berg-Purcell limit revisited. *Biophys. J.* 106:976–985.

59. Aquino, G., N. S. Wingreen, and R. G. Endres. 2016. Know the single-receptor sensing limit? Think again. *J. Stat. Phys.* 162:1353–1364.

60. Mora, T., and I. Nemenman. 2019. Physical limit to concentration sensing in a changing environment. *Phys. Rev. Lett.* 123:198101.

61. Hossain, S. S., S. F. A. Hossainy, …, T. J. R. Hughes. 2012. Mathematical modeling of coupled drug and drug-encapsulated nanoparticle transport in patient-specific coronary artery walls. *Comput. Mech.* 49:213–242.